Deep Neural Networks for Ultrasound Beamforming

Adam Luchies and Brett Byram
Department of Biomedical Engineering
Vanderbilt University
Nashville, TN, USA
adam.c.luchies@vanderbilt.edu

***Abstract*—We trained deep neural networks (DNNs) to suppress off-axis scattering. The networks operated on sub-band ultrasound channel data in the frequency domain and a different network was trained for each frequency. The in-phase and quadrature components of the signals were treated as separate inputs to the network and the output structure was the same as the input. An inverse short-time Fourier transform (ISTFT) was used to reconstruct channel data. Training data was generated using simulations and the training data consisted of the responses from individual point targets. Performance was compared to standard delay-and-sum (DAS) beamforming using simulated a point target and anechoic cyst and a physical phantom anechoic cyst.**

For a simulated point target, the side lobes when using the DNN approach were about 80 dB below those of standard DAS. For a 5 mm diameter simulated anechoic cyst, the contrast ratio (CR), contrast-to-noise ratio (CNR), and speckle SNR (SNRs) were 50.9 dB, 4.7 dB, and 1.71, respectively, for the DNN approach and 32.0 dB, 4.8 dB, and 1.78, respectively, for standard DAS. For a 5 mm diameter anechoic cyst in a physical phantom, the CR, CNR, and SNRs were 47.5 dB, 4.76 dB, and 1.73, respectively, for the DNN approach and 26.7 dB, 5.5 dB, and 1.99, respectively, for standard DAS.

Keywords—beamforming, off-axis scattering, deep neural networks, short-time Fourier transform

I. Introduction

In the past ten years, deep neural networks (DNNs) have achieved state-of-the-art performance when tackling problems in fields such as image processing, speech processing, and natural language processing [1]. More recently, DNNs have been applied to medical image processing problems and are just beginning to be examined for medical image reconstruction problems [2]. However, to our knowledge, DNNs have never been applied to ultrasound beamforming.

Our goal was to use DNNs during ultrasound beamforming to address the problem of acoustic clutter. Several sources of acoustic clutter, including off-axis scattering and reverberation, can degrade ultrasound image quality. Improving ultrasound image quality by reducing clutter would decrease the overall rate of ultrasound exam failure. After training, neural networks have fast execution times, particularly relative to similar approaches that rely on solving a nonlinear regression problem [3, 4].

II. Methods

We trained neural networks to suppress off-axis scattering. The training data was simulated using the FIELD II acoustic simulation software package and consisted of the responses from individual point targets [5]. The point targets were randomly located along an arc as shown in Fig. 1. The simulated array was modeled after an L7-4 linear array transducer. The scanning aperture had 65 elements on transmit and receive, the pitch was 298 μm, the kerf was 48 μm, and the transmit focal depth was 45 mm. The impulse response for the array elements was a Gaussian pulse with 5.208 MHz center frequency and 75% fractional bandwidth. The decimated sampling frequency was 20.832 MHz.

For a single point target, the time-domain signal was

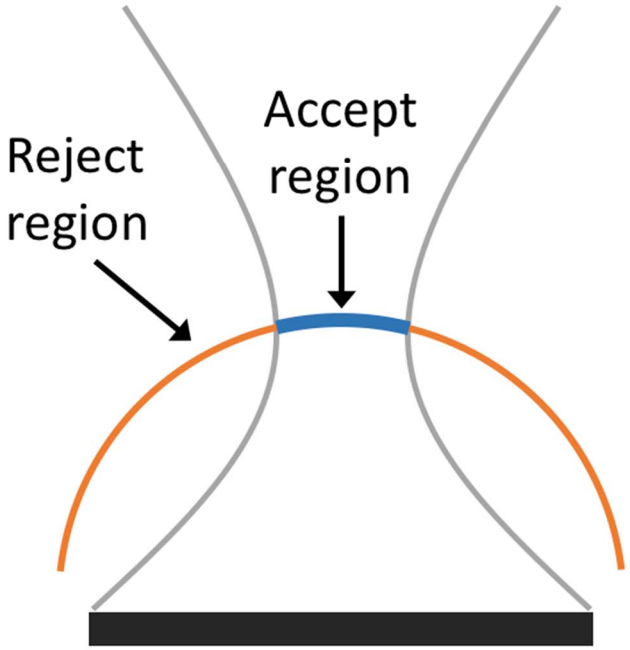

Fig. 1. Point targets were placed randomly along an arc.

The authors acknowledge the support of NIH R01EB020040.

XXX-X-XXXX-XXXX-X/XX/$XX.00 ©20XX IEEE

simulated using FIELD II and gated using window that had length of one pulse length. A fast Fourier transform (FFT) was used to convert the channel data to the frequency domain. A network was trained for the frequency bin associated with the center frequency of the transducer. This network was used as the starting point to train networks for the other frequency bins. Before inputting the data into a network, the in-phase and quadrature components were separated and treated as separate inputs to the same network.

We used fully-connected feed-forward neural networks with 130 inputs and the same number of outputs (i.e., two times the number of elements in the scanning aperture of the array). For signals from point targets in the acceptance region, the output vector was the same as the input vector. For point targets in the rejection region, the output vector was a vector of zeros.

We performed an extensive hyperparameter search to find good performing networks. The hyperparameter search space is shown in Table I. We selected the best performing network by creating a beam profile plot for each network and looking for the network with the best side lobe and gain performance. These metrics were also examined as a function of input scaling multiplier.

TABLE I. HYPERPARAMETER SEARCH

Parameter	**Value**
Hidden Layers	1-10
Layer Widths	100-1000
Learning Rates	10^{-6}, 10^{-5}, 10^{-4}, 10^{-3}, 10^{-2}
Dropout probability	0-0.5

We examined images for a simulated point target, a simulated anechoic cyst, and phatom anechoic cyst in order to compare the DNN approach to standard delay-and-sum (DAS) beamforming. For the anechoic cyst images, image quality was quantified using contrast ratio (CR), contrast-to-noise ratio (CNR), and speckle SNR.

III. RESULTS

Fig. 2 compares the simulated point target images using DAS and the DNN approach. The DNN approach suppressed the tails that are characteristic for DAS point target and that are clearly visible in Fig. 2 (a). The axially integrated lateral profile is in Fig. 2 (c) and shows that side lobes were suppressed by approximately 80 dB when using the DNN approach compared to standard DAS. The axial profile through the center of the point target is in Fig. 2 (d) shows that the axial response when using the DNN approach was slightly higher than that observed when using DAS. It is interesting to note that the worst axial responses were at transition between main lobe and side lobe regions. The result demonstrates that the DNN approach was able to suppress side lobes in a point target image.

Fig. 3 shows simulated cyst images produced using standard DAS and the proposed DNN approach. The CR, CNR, SNRs were 50.9 dB, 4.7 dB, and 1.71, respectively, for the DNN approach and 32.0 dB, 4.8 dB, and 1.78, respectively, for standard DAS. These results are noteworthy because the networks were trained on the responses from individual point targets and the networks produced an image of an anechoic cyst with improved contrast while preserving speckle.

Fig. 4 shows the physical phantom cyst images produced using standard DAS and the proposed DNN approach. The CR, CNR, and SNRs were 47.5 dB, 4.76 dB, and 1.73, respectively, for the DNN approach and 26.7 dB, 5.5 dB, and 1.99, respectively, for standard DAS. These results are noteworthy because the networks were trained using simulated data and the networks improved contrast while preserving speckle.

IV. CONCLUSIONS

We trained neural networks using simulated training data from individual point target responses and found that these networks increased contrast and preserved speckle for simulated and anechoic cyst. These results suggest the significant potential for training neural networks to operate on ultrasound channel to produce improvements in ultrasound image quality.

[1] I. Goodfellow, Y. Bengio, and A. Courville, Deep Learning, MIT Press, 2016.

[2] G. Wang, “A perspective on deep imaging,” IEEE Access, vol. 4, pp. 8914–8924, November 2016.

[3] B. Byram and M. Jakovljevic, "Ultrasonic Multipath and Beamforming Clutter Reduction: A Chirp Model Approach," IEEE Trans. Ultrason., Ferroelec., Freq. Contr., vol. 61, no. 3, pp. 428–440, 2014.

[4] B. Byram, K. Dei, J. Tierney, and D. Dumont, "A Model and Regularization Scheme for Ultrasonic Beamforming Clutter Reduction," IEEE Trans. Ultrason., Ferroelec., Freq. Contr., vol. 62, no. 11, pp. 1913–1927, 2015.

[5] J. A. Jensen and N. B. Svendsen, "Calculation of pressure fields from arbitrarily shaped, apodized, and excited ultrasound transducers," IEEE Trans. Ultrason., Ferroelec., Freq. Contr., vol. 39, pp. 262–267, 1992.

978-1-5386-3383-0/17/$31.00 ©2017 IEEE

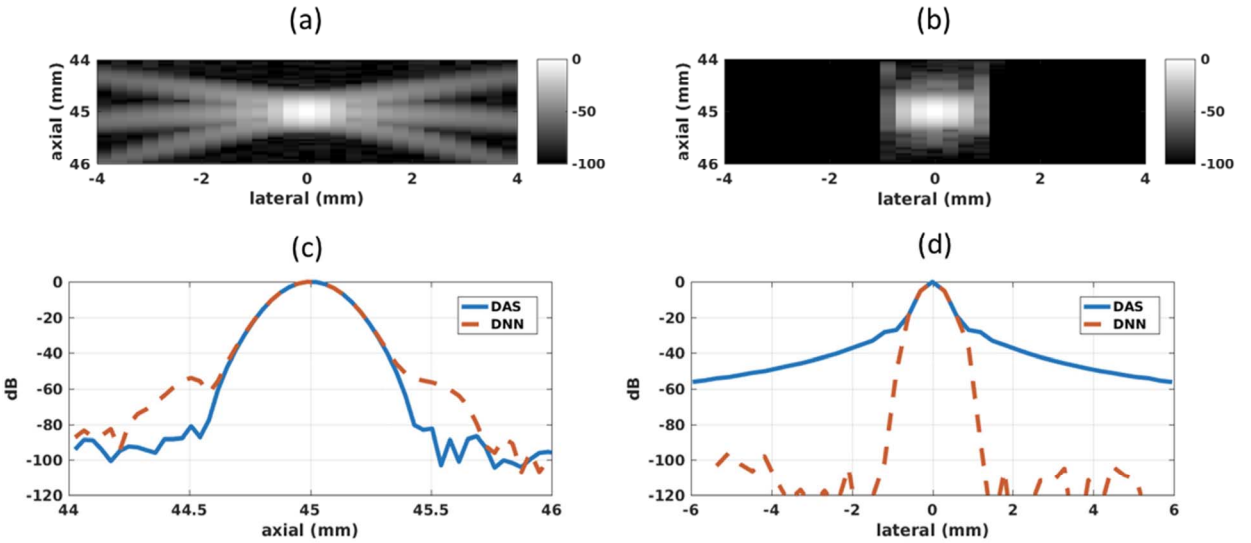

Fig. 3. Simulated point target using (a) standard delay-and-sum and (b) deep neural networks, (c) axial profile through the center of the target, and (d) axially integrated lateral profile at the focal depth.

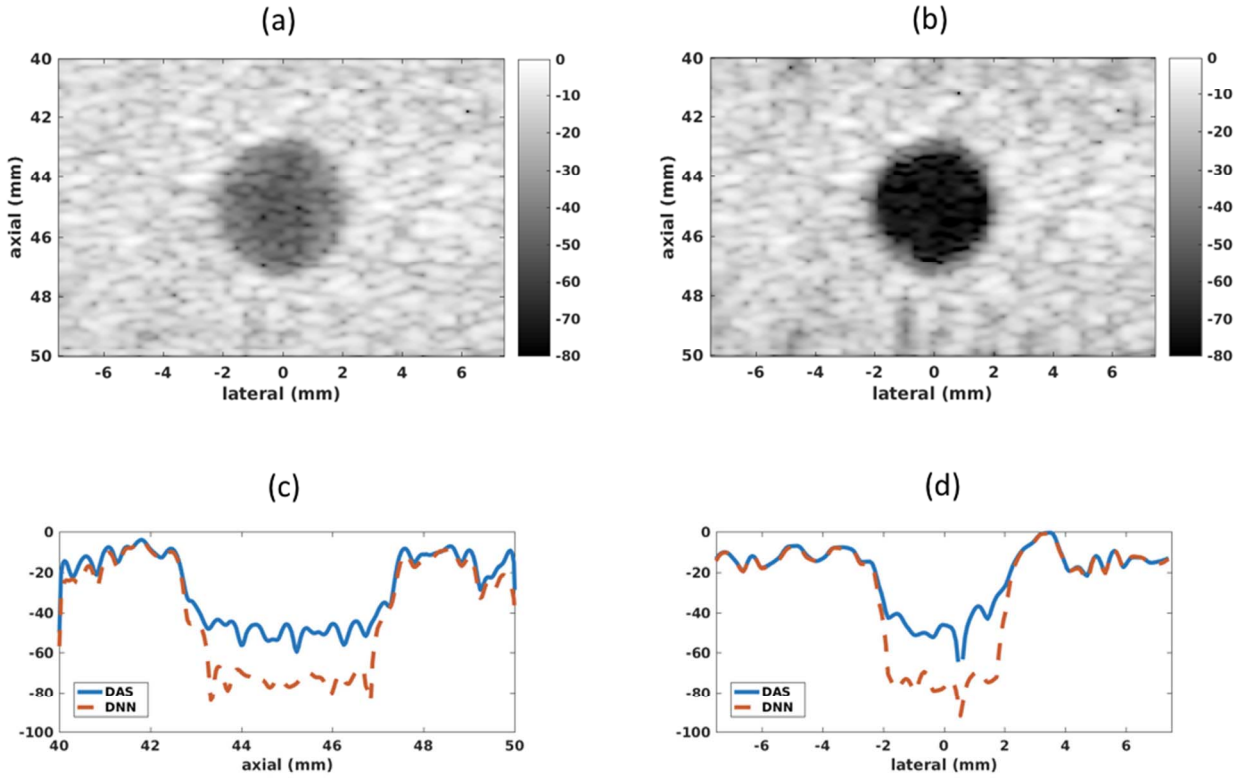

Fig. 2. Simulated anechoic cyst using (a) standard delay-and-sum and (b) deep neural networks, and (c) axial and (d) lateral profiles through the center of the cyst.

978-1-5386-3383-0/17/$31.00 ©2017 IEEE

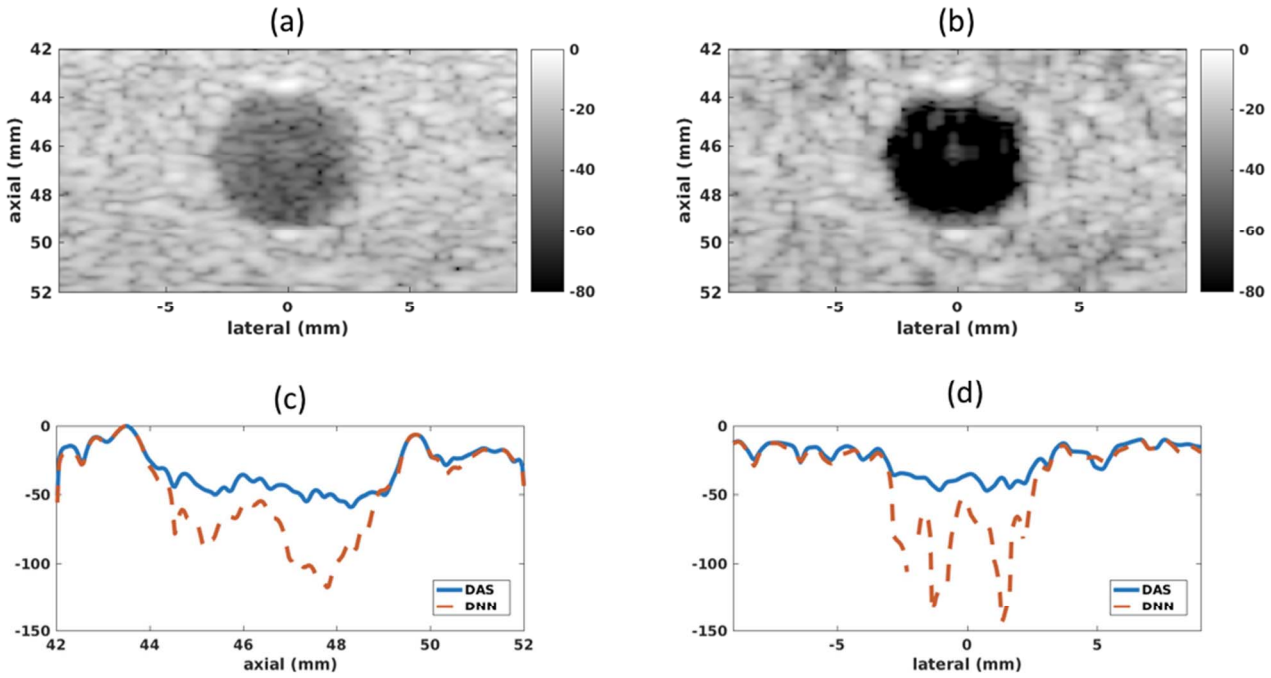

Fig. 4. Physical phantom anechoic cyst using (a) standard delay-and-sum and (b) deep neural networks, and (c) axial and (d) lateral profiles through the center of the cyst.

978-1-5386-3383-0/17/$31.00 ©2017 IEEE